Int. J. Heat Mass Transfer. Vol. 27, No. 5, pp. 739–746, 1984
Printed in Great Britain

0017-9310/84 $3.00 + 0.00
Pergamon Press Ltd.

AN ANALYTICAL SOLUTION OF THE HEAT TRANSFER PROCESS DURING MELTING OF AN UNFIXED SOLID PHASE CHANGE MATERIAL INSIDE A HORIZONTAL TUBE

M. BAREISS† and H. BEER

Institut für Technische Thermodynamik, Technische Hochschule Darmstadt, Petersenstrasse 30, 6100 Darmstadt, Federal Republic of Germany

(*Received* 30 *May* 1983)

Abstract – By means of a photograph technique the temporal geometric shape, melting rates and heat flux densities were determined experimentally. A force balance between pressure forces in a thin liquid layer between the bottom of the sinking solid bulk and the heated tubewall and the gravitational force of the solid bulk allows a closed-form solution of the melting process. Melting rates and heat transfer coefficients are in good agreement with the experiment.

NOMENCLATURE

- Ar Archimedes number
- C abbreviation
- c specific heat capacity
- F force
- g gravitational acceleration
- h_f specific latent heat of fusion
- k thermal conductivity
- L length of the tube
- m mass
- $\dot{m}$ mass flow rate
- Nu Nusselt number
- p pressure
- Pr Prandtl number
- $\dot{q}$ heat flux
- R_0 radius of the tube
- Ra Rayleigh number
- r radial coordinate
- s shift of the solid bulk
- s_0 apparent shift
- T temperature
- u velocity.

Greek symbols

- δ width of the molten gap
- δ_s thickness of the layer, melted from above
- η dynamic viscosity
- $\dot{\mu}$ mass flux
- ν kinematic viscosity
- ρ density
- τ time
- τ_a duration of the melting process
- ϕ angle of perimeter
- ϕ_A angular extent of the contact area.

Subscripts

- b buoyancy
- f fusion
- g gravitation
- l liquified
- p pressure
- s solid
- tot total
- w wall.

Superscripts

- $\bar{}$ mean value
- * dimensionless quantity.

INTRODUCTION

MELTING and fusion phenomena take place in numerous technical and natural processes. In recent years latent heat storage systems have gained importance for many applications in room heating and heat recovery systems, because of their high energy density and isothermal behaviour during charging and discharging. As a consequence, many papers have been published in recent years concerning melting and fusion phenomena in various configurations. The majority of the publications report on experimental investigations for different geometries. Heat transfer phenomena accompanying the phase change process above or below a heated horizontal flat plate and at a vertical surface were studied by Hale and Viskanta [1, 2], whereas the influence of the height of the heated surface has been investigated over a wide range by Bareiss *et al.* [3].

Another important arrangement for technical application—the phase change process around a single or an array of horizontal cylinders (finned and unfinned)—was the subject of several experimental investigations [4–8]. Rieger *et al.* [9] were successful in solving this problem numerically. The melting process inside cylindrical enclosures has been studied extensively as well. The vertical arrangement was investigated experimentally by Bareiss and Beer [10] and the horizontal configuration was the subject of numerical [11, 12], experimental [13] and both, numerical and experimental [14] studies. The common feature of the aforementioned investigations with regard to the melting process inside a horizontal heated tube is the solid phase change material (PCM) being

† Present address: Battelle-Institut, D6000 Frankfurt, Federal Republic of Germany.

fixed at its position during melting. Under this condition, the melting process shows a typical behaviour. In the earliest stage of the process the heat transport is controlled by heat conduction only, thus causing an axisymmetrical annular gap of molten PCM adjacent to the heated wall. With proceeding time and increasing width of the gap, convective fluid motions set in. As a result of the local orientation of the convective heat transfer mechanism, the motion and the shape of the liquid–solid interface loses its axisymmetrical characteristic. It is evident, that the melting process will show a quite different behaviour, if the solid PCM is unfixed and therefore allowed to sink to the bottom of the cylinder, following a gravitational force resulting from the difference between solid and liquid density. Taking account of this phenomenon, Nicholas and Bayazitoglu [15] performed a numerical analysis by solving the governing equations with the aid of a finite-difference method. The results of their experiments are used for qualitative purposes only and unfortunately no comparisons with the theoretical results are presented. Within the compass of the work presented in this paper, a number of experiments were performed, covering a wide range of the governing parameters. A closed-form solution, which could be obtained via a theoretical analysis of the melting process, shows excellent agreement with the experimental results.

EXPERIMENTS

Test apparatus

The test apparatus (Fig. 1) consists of a copper tube (1) of 40 mm in length, 32 resp. 60 mm I.D. and a wall thickness of 1 mm. The copper tube is closed at one end by a firmly adhered, 10 mm thick circular Plexiglas disk (2a). A second Plexiglas disk (2b) is held on the other end by a special adhesive, which allows the disk to be released if necessary. Thus a horizontal cylindrical space of 32 resp. 60 mm diameter and 40 mm length is formed which contains the PCM. Since the cell is translucent in the axial direction a visual observation and photographic registration of the melting process is possible. Through the annular gap between the copper tube and the outer cylindrical jacket (3) water acting as a heating or cooling fluid can be circulated. The water is supplied by a constant temperature thermostat through an inlet tube (4) tangentially to the annular gap. By this means high heat transfer rates and therefore constant surface temperature conditions at the wall of the copper tube can be achieved. Since the temperature drop across the copper tube wall is less than 0.02 K, the temperature of the inside surface of the wall can be assumed to be equal to that of the outside surface. For the measurement of the wall temperature T_w, thermocouples therefore could be cemented in small grooves and covered with thin copper foil on the outside surface. The volumetric expansion of the PCM during melting is compensated by an overflow pipe (5).

Phase change material

Both $C_{18}H_{38}$, n-octadecane ($Pr = 50$, $h_f = 243$ kJ kg^{-1}, $T_f = 301.2$ K) and C_9H_{10}, *p*-xylene ($Pr = 8.5$, $h_f = 161$ kJ kg^{-1}, $T_f = 286.4$ K) were chosen as test materials because the melting temperatures are close to the ambient temperature and since they are non-toxic, noncorrosive and transparent in the liquid phase. The physical and transport properties are well established. The data used in this study were taken from Hale *et al.* [16] and Vargaftik [17].

Test procedure

Since n-octadecane and *p*-xylene possess a high dissolving capacity for air, the test material must be degassed carefully prior to each experiment. For this purpose the test material was subjected to a

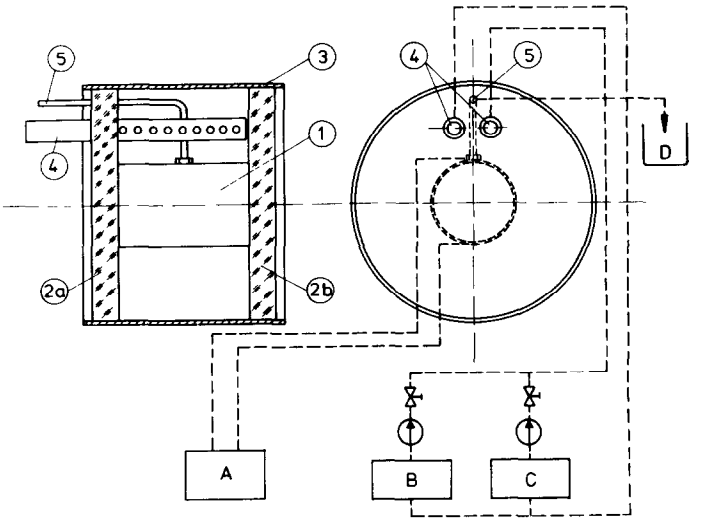

FIG. 1. Test apparatus: (1) copper tube; (2a), (2b) Plexiglas disk; (3) outer cylinder; (4) inlet tube; (5) overflow pipe.

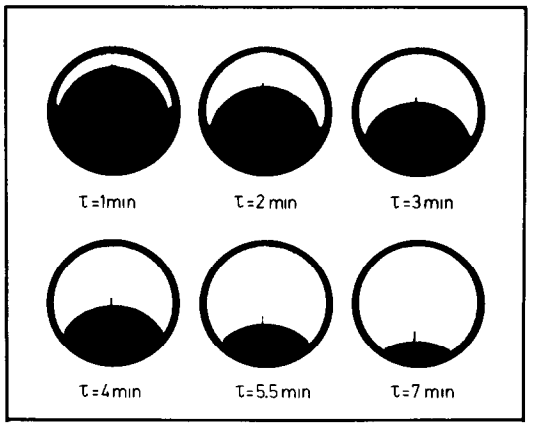

FIG. 2. Melting process represented by a sequence of photographs.

solidification–melting cycle under vacuum. The opened test cell was lengthened by an additional copper tube attached to the open end and then filled with the degassed liquid PCM. The assembly was placed vertically into an icewater bath to solidify the PCM. After solidification, the lengthening tube was detached, the excess of solid PCM cut off and the cross-sectional area carefully planed. By this means a void-free and homogeneous solid could be obtained in the test cell. After the test cell was closed and assembled, the PCM was heated to a steady temperature, 0.5 K below the melting point at the most by circulating water. During the test itself, which starts when the copper tube wall is suddenly heated to a desired temperature above the melting point, the process was registrated photographically. For this purpose photographs were taken at selected time intervals with a telelens camera.

Melting phenomena

A typical melting process is shown in a sequence of photographs in Fig. 2. Because of its higher density the unfixed solid bulk (black area) sinks to the bottom of the tube. This behaviour results in a good thermal contact and, as a consequence, in an intensive melting process along the contact area. As evidenced by Fig. 2, the essential feature of the considered process is a downward motion of the solid bulk. Surprisingly the upper interface of the solid bulk maintains its circular shape during the entire process. Nevertheless, melting occurs at this upper interface too, as documented by the setting free of the pin at the top of the solid bulk. Prior to the test, this pin was embedded in the solid material adjacent to the tube wall. Therefore, the length of the pin corresponds directly to the thickness of the solid layer liquified at this point. An analysis of the experiments yields, that 10–15% of the total PCM mass only melts at the upper solid–liquid interface. Moreover, the shape of this interface does not change and can be well approximated by a circular arc with invariable curvature throughout the entire process. This fact is due to the pattern of the convective fluid motions in the fluid bulk above the solid material.

Along the contact area, a very thin molten gap between solid bulk and heated tube wall must exist, though it is impossible to detect it photographically. Within this gap the molten material flows as a coherent film-like fluid layer to the edge of the contact area. These conditions indicate, that the pressure inside this layer causes the bearing force for the solid bulk.

In order to analyse the experiments, it is reasonable to characterize the melting process with the aid of two quantities, determined as a function of time. These quantities are the thickness δ_s of the molten layer at the top of the molten bulk and the downward shift s of a solid-fixed point. In Fig. 3 these quantities are plotted against the time for one selected test.

It is evident, that the quantity s, which corresponds to the melting rate at the contact area, is considerably larger than δ_s. Further, the increase of δ_s with time shows a quite linear behaviour, whereas the slope of the s–τ, curve decreases with time.

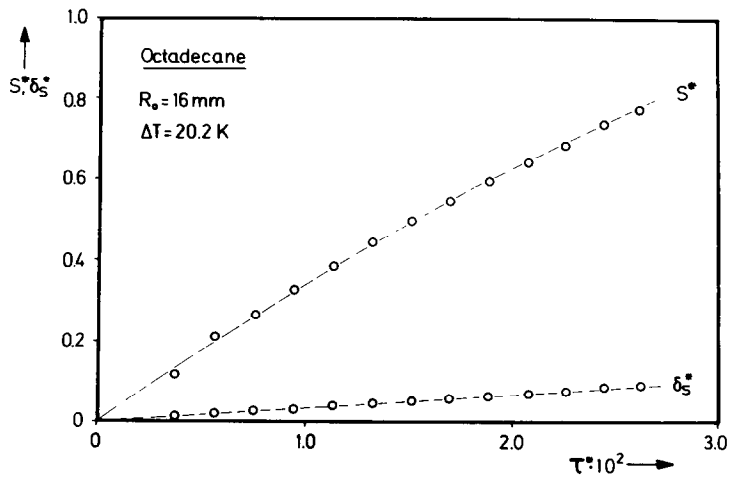

FIG. 3. Shift, s^*, of the solid bulk and thickness, δ_s^*, of the molten layer as a function of the dimensionless time, τ^*.

Analysis

In order to describe the melting process the geometric quantities depicted in Fig. 4 are introduced. As mentioned, the downward motion of the solid bulk is characterized by the time dependent shift of s of a material-fixed reference point M_f, which is chosen to be the centre of the originally cylindrical solid bulk. At the beginning of the melting process ($\tau = 0$) M_f coincides therefore with the axis M_c of the tube. The angle of the perimeter is denoted with ϕ and the extent of the contact area is measured by ϕ_A.

Taking into account the aforementioned fact, that the shape of the upper solid–liquid interface is a circular arc with invariable radius R_0 throughout the entire process, the actual cross-sectional area of the solid bulk can be assumed to result from superposing the shift s with an apparent shift δ_s to a total value s_0

$$s_0 = s + \delta_s. \tag{1}$$

It is advantageous, to introduce the dimensionless geometric quantities

$$s_0^* = \frac{s_0}{2R_0}, \quad s^* = \frac{s}{2R_0}, \quad \delta_s^* = \frac{\delta_s}{2R_0}, \tag{2}$$

and the dimensionless time

$$\tau^* = Ste\,Fo = \frac{c_l \Delta T}{h_f}\frac{a_l \tau}{R_0^2}, \tag{3}$$

as a product of the Stefan and Fourier numbers.

The molten mass fraction can be evaluated from the cross-sectional area of the solid bulk

$$m_f^* = \frac{m_l}{m_{tot}} = \frac{\arcsin s_0^* + s_0^*\sqrt{(1-s_0^{*2})}}{\pi/2}. \tag{4}$$

The basis of the following analysis is a balance of forces at the melting solid bulk. As pointed out, the pressure forces in the thin liquid layer between its bottom interface and the heated tubewall bear the solid bulk.

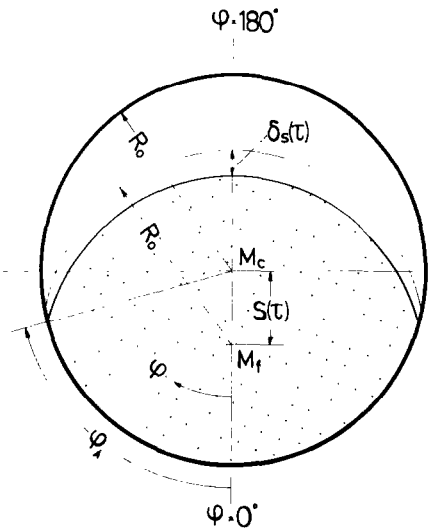

FIG. 4. Representation of geometric quantities.

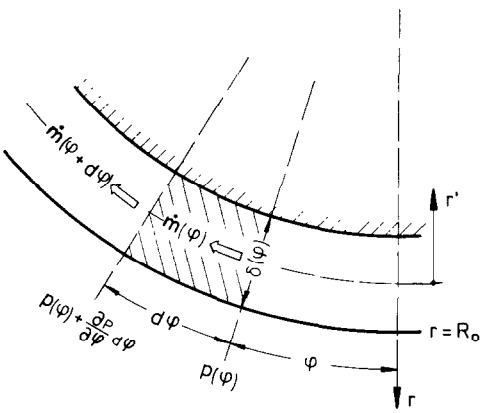

FIG. 5. Schematic representation of the physical model.

Under the assumption of a quasi-steady downward motion of the bulk, inertial forces can be neglected.

Therefore, the acting forces are balanced, when the vertical resultant of the pressure forces is equal to the value of the difference between the gravitational and buoyancy forces of the solid bulk

$$F_p = F_g - F_b. \tag{5}$$

That is, in terms of the acting forces

$$\frac{1}{R_0}\int_{\phi=0}^{\phi_A} p(\phi)\cos\phi\,\mathrm{d}\phi = g(\rho_s - \rho_l)[\arccos s_0^* - s_0^*\sqrt{(1-s_0^{*2})}], \tag{6}$$

where ρ_s and ρ_l are the density of the solid and liquid PCM, respectively, and $p(\phi)$ is the pressure distribution inside the bearing liquid layer. In order to determine this *a priori* unknown pressure distribution the model depicted in Fig. 5 is used.

Due to the melting process at the solid–liquid interface, characterized by the mass flux $\dot{\mu}(\phi)$ of the molten PCM, the mass flow rate in the gap will increase with the angular coordinate ϕ. It is evaluated from

$$\dot{m}(\phi) = LR_0\int_0^{\phi}\dot{\mu}(\phi)\,\mathrm{d}\phi. \tag{7}$$

Within the considered gap-element, the mass flow rate $\dot{m}(\phi)$ is assumed to be invariable and will correspond to the local pressure gradient $\partial p/\partial\phi$. In order to quantify this relation, the following simplifying assumptions are made:

(1) the fluid flow within the gap is quasi-steady and laminar;

(2) pressure gradients and fluid velocities in the radial direction are non existent;

(3) body forces are neglectable;

(4) the density of the fluid is constant.

With these in mind, the conservation equations in cylindrical coordinates can be written as

$$\frac{\partial u}{\partial\phi} = \frac{\partial^2 u}{\partial\phi^2} = 0, \tag{8}$$

for the mass

$$-\rho_l \frac{u^2}{r} = 0, \tag{9}$$

for the momentum in the r-direction and

$$\eta \frac{\partial^2 u}{\partial r^2} = \frac{1}{r}\frac{\partial p}{\partial \phi}, \tag{10}$$

for the momentum in the ϕ-direction.

From equations (7)–(10), an expression for the local pressure gradient can be derived

$$\frac{dp}{d\phi}(\phi) = -\frac{12\eta R_0}{\rho_l}\frac{1}{\delta^3(\phi)}\int_0^{\phi} \dot{\mu}(\phi)\,d\phi. \tag{11}$$

In this expression the distribution of the local mass flux $\dot{\mu}(\phi)$ as well as the local width $\delta(\phi)$ of the gap are unknown *a priori*. It is justified to assume that the heat transport from the heated wall to the melting PCM across the liquid layer is controlled by conduction. Then a heat balance at the solid–liquid interface yields the following correlation between the mass flux $\dot{\mu}(\phi)$ and the local width $\delta(\phi)$ under the condition of a linear temperature gradient across the gap

$$h_f \dot{\mu}(\phi) = \frac{k_l}{\delta(\phi)}(T_w - T_f). \tag{12}$$

The heat absorbed by the phase change process at the solid–liquid interface is equal to the heat supply by conduction. The fraction of the heat flux spent for the increase of the sensible heat of the molten material is neglected here, nevertheless, it can easily be taken into account by an apparently increased latent heat

$$h_f' = h_f + c_l(T_w - T_f)/2,$$

if necessary.

Beyond that, the local mass flux $\dot{\mu}$ is subjected to a kinematic condition. At any arbitrary position along the contact area, the value of $\dot{\mu}(\phi)$ must allow the solid bulk to sink with a downward velocity $\dot{s} = ds/d\tau$

$$\dot{\mu}(\phi) = \rho_s \dot{s}\cos\phi. \tag{13}$$

With the aid of equations (12) and (13) the pressure distribution in the gap can be determined by integration of equation (11)

$$p(\phi) = 3\eta R_0^2 \rho_s^4 \left(\frac{h_f}{k_L(T_w - T_f)}\right)^3 \times (\cos^4\phi - \cos^4\phi_A)\dot{s}^4. \tag{14}$$

With regard to this equation and using $\cos\phi_A = s_0^*$, a relation for the downward velocity of the solid bulk can be derived from the balance of forces [equation (6)]. Introducing dimensionless parameters finally results in

$$\frac{ds^*}{d\tau^*} = 0.402\left(\frac{Pr}{Ste}Ar\,\rho^{*3}\right)^{1/4} \times \left[\frac{\arccos s_0^* - s_0^*\sqrt{(1-s_0^{*2})}}{\sqrt{(1-s_0^{*2})}(2/3 + s_0^{*2}/3 - s_0^{*4})}\right]^{1/4}. \tag{15}$$

Here Ar denotes the Archimedes number

$$Ar = \frac{\rho_s - \rho_L}{\rho_s}\frac{gR_0^3}{\nu^2},$$

a parameter, which corresponds to the apparent weight, the difference between the gravitational and buoyancy forces of the solid bulk. In order to obtain a simple but nevertheless accurate solution, two approximations are introduced. First, the transcendental function within the square bracket of equation (15) can be substituted with a vanishing error by a second-order polynomial. Then equation (15) (inverted) changes to

$$\frac{d\tau^*}{ds^*} = 2.49\left(\frac{Ste}{Pr\,Ar}\right)^{0.25} \times \rho^{*-0.75}(0.81 + 0.27s_0^* + 0.18s_0^{*2}). \tag{16}$$

Taking into account that

$$s_0^*(\tau) = s^*(\tau) + \delta_s^*(\tau),$$

the differential equation, equation (16), can be integrated provided that the function $\delta_s^*(\tau)$ respectively $\delta_s^*(s^*)$ is available. As already pointed out, the melting process at the upper interface of the solid bulk is of secondary importance. Therefore, a simple empirical approximation seems to be adequate

$$Nu|_{\phi=180°} = c_l Ra^{0.25}. \tag{17}$$

This expression for the local Nusselt number is of physical significance, because the melting process at the upper interface is controlled by convective heat transfer as indicated by the experiments. They yield $c_l = 0.2$.

With

$$Nu|_{180°} = \frac{2}{\rho^*}\frac{d\delta_s^*}{d\tau^*},$$

as the defining equation

$$\delta_s^* = 0.1\rho^*\,Ra^{0.25}\,\tau^*, \tag{18}$$

follows from equation (17). In order to eliminate the dependency on time, an approximate but adequate correlation between τ^* and s^* can be derived from equation (16). Finally

$$s_0^* = s^*(1 + C), \tag{19}$$

results, where the abbreviation

$$C = 0.25\left(Ste\,\rho^*\frac{Ra}{Pr\,Ar}\right)^{0.25}, \tag{20}$$

as the ratio of δ_s^* to s^* quantifies the proportion of both melting mechanisms. With these relations, a solution of equation (16) can easily be obtained

$$\tau^* = 2\left(\frac{Ste}{Pr\,Ar}\right)^{0.25}\rho^{*-0.75}\left(\frac{1}{1+C}\right) \times (s_0^* + 0.167s_0^{*2} + 0.074s_0^{*3}). \tag{21}$$

Considering the definition of s_0^*, it is evident, that the PCM inside the tube is completely liquified, when

$s_0^* = 1.0$. The elapsed time

$$\tau_a^* = 2.49\left(\frac{Ste}{Pr\,Ar}\right)^{0.25}\rho^{*-0.75}\left(\frac{1}{1+C}\right), \quad (22)$$

is the duration of the complete melting process and obviously corresponds to the group of dimensionless parameters in equation (21). With this abbreviation, the mentioned equation may be rewritten as

$$\tau^* = 0.805\tau_a^*(s_0^* + 0.167s_0^{*2} + 0.074s_0^{*3}). \quad (23)$$

As already pointed out, the heat transport is dominated by conduction. Nevertheless it is advantageous to introduce a Nusselt number in order to describe this process. With the heat flux averaged with respect to the area of the heated tube wall and referred to the temperature difference $\Delta T = T_w - T_s$, an averaged Nusselt number can be defined as

$$\overline{Nu} = \frac{(\bar{q}/\Delta T)R_0}{k_l}. \quad (24)$$

As the heat flow rate corresponds to the mass melting per unit time, the introduced Nusselt number can be evaluated from this measurable quantity

$$\overline{Nu} = \frac{1}{2\rho^*}\frac{dm_l^*}{d\tau^*}. \quad (25)$$

Via equations (4) and (21), a closed-form expression of the dimensionless melting rate and hence the averaged Nusselt number is derived

$$\overline{Nu} = \overline{Nu}\frac{\sqrt{(1-s_0^{*2})}}{(0.63+0.21s_0^*+0.14s_0^{*2})}. \quad (26)$$

Here

$$\overline{Nu} = 0.2\left(\frac{Pr\,Ar}{Ste}\right)^{0.25}\rho^{*-0.25}(1+C), \quad (27)$$

accounts for a mean dimensionless melting rate

$$\left(\frac{dm_l^*}{d\tau^*}\right) = \frac{1}{\tau_a^*}, \quad (28)$$

and denotes the Nusselt number, averaged as well with respect to the area of the tube wall as with respect to the melting duration τ_a^*. Using equations (19) and (22)–(27), a set of relations is available for calculating all important characteristics of the considered melting process.

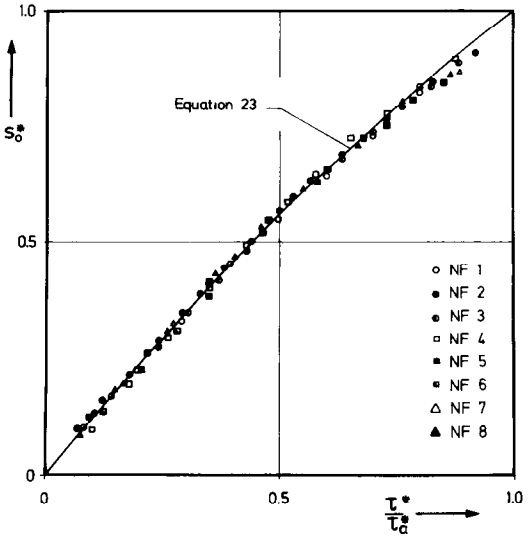

FIG. 6. Total shift, s_0^*, as function of the related, dimensionless time.

COMPARISON WITH EXPERIMENTAL RESULTS AND DISCUSSION

Equation (23), in combination with equations (19) and (20), describes the downward motion of the solid bulk inside the horizontal tube. In Fig. 6 the total shift s_0^* is plotted against the related dimensionless time τ^*/τ_a^*. The characterization of the measured data points refers to the numbers of the performed experiments summarized in Table 1. It is evident, that equation (23) agrees very well with the experimental results. The measured data show some deviation only in the final period of the melting process, resulting in an insignificant deceleration of the downward motion of the solid bulk. This reduction in accuracy of the theoretical model accounts for its inherent fundamentals. The assumption of quasi-steady hydrodynamic phenomena within a melting gap of quasi-steady geometry fails in the final stage of the process, when the length of the gap is subjected to a fast decrease, due to geometric constraints. In Fig. 7 $\overline{Nu}/\overline{Nu}$ is plotted against the total shift s_0^*, according to equation (26). The theoretical and experimental data show a very good agreement, similar to the preceding representation. Figure 7 indicates, that the heat transfer characterized

Table 1. Parameters of the performed experiments

Number of test	R_0 [mm]	ΔT [K]	*Ste*	*Ar*	*Pr*	Test material
NF 1	30	10.1	0.09	$6.8 \cdot 10^5$	49.5	octadecane
NF 2	30	6.5	0.058	$6.25 \cdot 10^5$	50.9	octadecane
NF 3	30	20.1	0.18	$8.7 \cdot 10^5$	45.7	octadecane
NF 4	16	19.9	0.18	$1.3 \cdot 10^5$	45.8	octadecane
NF 5	16	9.2	0.081	$1.0 \cdot 10^5$	49.9	octadecane
NF 6	30	10.2	0.105	$8.1 \cdot 10^7$	8.15	*p*-xylene
NF 7	16	9.9	0.105	$1.2 \cdot 10^7$	8.15	*p*-xylene
NF 8	16	5.1	0.05	$1.1 \cdot 10^7$	8.30	*p*-xylene

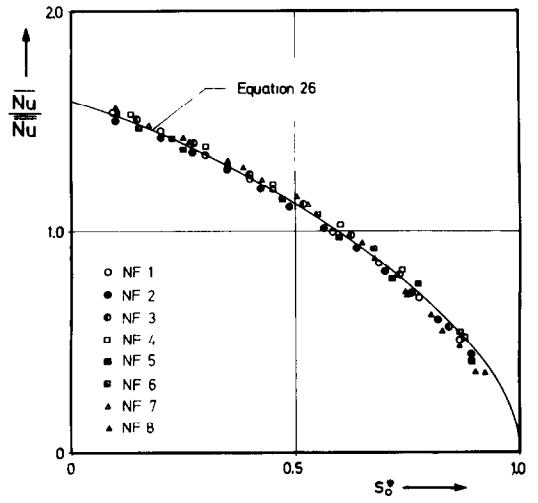

FIG. 7. Related Nusselt number as function of the total shift, s_δ^*.

with respect to equation (24) by the Nusselt number $\overline{Nu}$, is a maximum at the beginning and decreases monotonically to zero at the end of the melting process. This behaviour is due to the decreasing contact—heat transfer—area of the melting solid bulk. With the aid of equation (27) a significant characteristic of the considered melting process can be verified. In contrary to the natural convection controlled heat transfer mechanism, the introduced 'heat transfer coefficient' $\bar{q}/\Delta T$ decreases with increasing temperature difference ΔT. Mathematically, this is due to the reciprocal influence of the Stefan number, which is formed with ΔT. Physically this behaviour results from the melting gap, whose thickness and hence heat resistance increases with increasing melting rate.

CONCLUSION

The solution of the analytical model of the melting process, though derived with the aid of a number of approximate assumptions, agrees very well with the experimental results. As the covered range of test parameters was restricted, it is necessary, however to define the limits of validity of the analytical solution. Equations (21) and (27) were derived under the implicit condition, that the quantity C [equation (20)] is small compared to 1. As mentioned, this quantity denotes the ratio of δ_s^* to s^* and therefore relates the melting rate from above to that from below. It is explained by equation (20) that the value of C increases with increasing temperature difference ΔT and therefore can exceed the above-mentioned magnitude. With the aid of these considerations, the limit of validity of the analytical solution can be defined by means of the following expression

$$Ste\,\rho^* \frac{Ra}{Pr\,Ar} < 1.4. \qquad (29)$$

With respect to the test materials as well as to the majority of the existing phase change heat storage materials this criterion limits the application of the given solution to temperature differences $\Delta T \leqslant 60$–100 K. Latent heat storage conditions afford much smaller temperature differences.

Acknowledgements—The authors wish to express their appreciation for the support of this work by the Deutsche Forschungsgemeinschaft—DFG.

REFERENCES

1. N. W. Hale, Jr. and R. Viskanta, Solid–liquid phase change heat transfer and interface motion in materials cooled or heated from above and below, *Int. J. Heat Mass Transfer* **23**, 283–292 (1980).
2. N. W. Hale, Jr. and R. Viskanta, Photographic observation of the solid–liquid interface motion during melting of a solid heated from an isothermal vertical wall, *Lett. Heat Mass Transfer* **5**, 329–337 (1978).
3. M. Bareiss, T. Betzel and H. Beer, Melting from a vertical wall. Influence of different wall heights and temperature differences on heat transfer and interfacial motion, University Report, Darmstadt (1980).
4. R. D. White, A. G. Bathelt and R. Viskanta, Study of heat transfer and melting from a cylinder embedded in a phase change material, ASME Paper No. 77-HT-42 (1977).
5. A. G. Bathelt, R. Viskanta and W. Leidenfrost, Latent heat of fusion energy storage, experiments on heat transfer from cylinders during melting, *J. Heat Transfer* **101**, 453–458 (1979).
6. A. G. Bathelt and R. Viskanta, Heat transfer at the solid–liquid interface during melting from a horizontal cylinder, *Int. J. Heat Mass Transfer* **23**, 1493–1503 (1980).
7. R. Viskanta, A. G. Bathelt and N. W. Hale, Latent heat-of-fusion energy storage: experiments on heat transfer during solid–liquid phase change, *Proc. 3rd Int. Conf. on Alternative Energy Sources*, Bal Harbour, Florida (1980).
8. R. J. Goldstein and J. W. Ramsey, Heat transfer to a melting solid with application to thermal energy storage systems, in *Heat Transfer Studies: a Festschrift for E.R.G. Eckert* (edited by J. P. Hartnett), pp. 199–206. Hemisphere, Washington, DC (1979).
9. H. Rieger, U. Projahn and H. Beer, Analysis of the heat transport mechanisms during melting around a horizontal circular cylinder, *Int. J. Heat Mass Transfer* **25**, 137–147 (1982).
10. M. Bareiss and H. Beer, Influence of natural convection on the melting process in a vertical cylindrical enclosure, *Lett. Heat Mass Transfer* **7**, 329–338 (1980).
11. J. Pannu, G. Joglekar and P. A. Rice, Natural convection to cylinders of phase change material used for thermal storage, *A.I.Ch.E. Symp. Ser.* 47–55 (1980).
12. T. Saitoh and K. Hirose, High Rayleigh number solutions to problems of latent heat thermal energy storage in a horizontal cylinder capsule, *J. Heat Transfer* **104**, 545–553 (1982).
13. K. Katayama, A. Saito, Y. Utoka, A. Saito, H. Matsu, H. Mae Kawa and A. Saifullah, Heat transfer characteristics of the latent heat thermal energy storage capsule, *Solar Energy* **27**, 91–97 (1981).
14. H. Rieger, U. Projahn, M. Bareiss and H. Beer, Heat transfer during melting inside a horizontal tube, *J. Heat Transfer* **105**, 226–234 (1983).
15. D. Nicholas and Y. Bayazitoglu, Thermal storage of a phase change material in a horizontal cylinder, *Proc. 3rd Int. Conf. on Alternative Energy Sources*, Bal Harbour, Florida (1980).
16. D. V. Hale, M. J. Hoover and M. J. O'Neil, *Phase Change Material Handbook*, NASA-CR-61363 (1971).
17. N. B. Vargaftik, *Tables on the Thermophysical Properties of Liquids and Gases*. Hemisphere, Washington, DC (1975).

SOLUTION ANALYTIQUE DU TRANSFERT THERMIQUE PENDANT LA FUSION D'UN MATERIAU SOLIDE DANS UN TUBE HORIZONTAL

Résumé—Au moyen d'une technique photographique, la forme géométrique instantanée, les vitesses de fusion et les densités de flux thermique sont déterminées expérimentalement. On obtient une solution analytique du problème à partir du bilan de forces, dans une fine couche liquide limitée par la base du noyau du solide noyé et la paroi du tube chaud, entre les forces de pression et la force gravitationnelle sur le solide. Les vitesses de fusion et les coefficients de transfert thermique sont en bon accord avec les expériences.

EINE ANALYTISCHE LÖSUNG ZUR WÄRMEÜBERTRAGUNG BEIM SCHMELZEN EINES NICHT FIXIERTEN FESTKÖRPERS IM WAAGRECHTEN ROHR

Zusammenfassung—Mit Hilfe einer photographischen Methode werden die geometrische Form des Schmelzkörpers, Schmelzraten und damit Wärmeubergangskoeffizienten in zeitlicher Abhängigkeit experimentell ermittelt. Auf der Basis eines Kräftegleichgewichts zwischen Druckkräften in einem dünnen Schmelzspalt zwischen Rohrwand und Unterseite des absinkenden Festkörpers und der Gewichtskraft des Festkörpers, gelingt eine geschlossene analytische Lösung zur Ermittlung der Schmelzraten sowie des Wärmetransportes, die eine gute Übereinstimmung mit Experimenten zeigt.

АНАЛИТИЧЕСКОЕ РЕШЕНИЕ ЗАДАЧИ ТЕПЛОПРОВОДНОСТИ ПРИ ПЛАВЛЕНИИ ТВЕРДОГО МАТЕРИАЛА С НЕУСТАНОВИВШЕЙСЯ ТОЧКОЙ ФАЗОВОГО ПЕРЕХОДА ВНУТРИ ГОРИЗОНТАЛЬНОЙ ТРУБЫ

Аннотация—Методом фотографирования проведено экспериментальное определение текущей геометрической формы, скоростей плавления и плотностей теплового потока. С помощью балансных соотношений между силами давления в тонком слое жидкости, расположенном между основанием твердого тела и нагреваемой стенкой трубы, и силой тяжести твердого тела для процесса плавления получено решение в замкнутой форме. Рассчитанные значения скоростей плавления и коэффициентом теплопроводности хорошо согласуются с экспериментальными данными.